Central Impurity Toroidal Rotation in ICRF Heated Alcator C-Mod Plasmas

J. E. Rice, P. T. Bonoli, J. A. Goetz, M. J. Greenwald,
I. H. Hutchinson, E. S. Marmar, S. M. Wolfe, S. J. Wukitch
Plasma Science and Fusion Center, MIT, Cambridge, MA 02139-4307

and

C. S. Chang
Courant Institute, NYU

Abstract

Central impurity toroidal rotation has been observed in Alcator C-Mod ICRF heated plasmas, from the Doppler shifts of argon x-ray lines. Rotation velocities up to 1.3×10^5 m/s in the co-current direction have been observed in H-mode discharges that had no direct momentum input. There is a strong correlation between the increase in the central impurity rotation velocity and the increase in the plasma stored energy, induced by ICRF heating, although other factors may be involved. This implies a close association between energy and momentum confinement. Co-current rotation is also observed during purely Ohmic H-modes. In otherwise similar discharges with the same stored energy increase, plasmas with lower current rotate faster. For hydrogen minority [D(H)] heating, plasmas with the highest rotation have an H/D ratio between 5 and 10 %, and have the resonance location in the inner half of the plasma, the same conditions conducive to the best ICRF absorption and heating. Comparisons with neo-classical theory indicate that the ion pressure gradient is an unimportant contributor to the central impurity rotation and the presence of a substantial core radial electric field is inferred during the ICRF pulse. An inward shift of ions induced by ICRF waves could give rise to a non-ambipolar electric field in the plasma core.

I. Introduction

Plasma rotation plays an important role in the transition from L- to H-mode in tokamak plasmas [1-4], and is associated with the formation of transport barriers. Poloidal rotation in the edge plasma region has been closely associated with the L-H transition [5-7], and toroidal momentum confinement is well correlated with energy confinement [8-11]. Whether the rotation is a cause or effect of the L-H transition remains an open question. Most observations of rotation [8-25] have been made in plasmas with an external momentum source, usually provided by neutral beams. The radial electric field, E_r, has been inferred from measured impurity rotation and the force balance equation [8,11,17,22-25]; a recent comprehensive review may be found in Ref.[26]. It is difficult to separate the contribution to the rotation from the direct momentum input of the neutral beams and the rotation that may be associated with (or induced by) H-modes, although some information has been obtained from balanced or perpendicular beam injection [8,11]. Toroidal impurity rotation in ohmic plasmas (no net momentum input) is consistent with neoclassical predictions [15,27,28]; in ohmic L-mode discharges, impurities rotate in the direction opposite to the plasma current [8,15,27,29,30]. In some neutral beam plasmas with ICRF heating, the rotation has been seen to drop significantly during the RF pulse [12]. Counter-current toroidal rotation associated with ion orbit loss in neutral beam and ICRF heated plasmas has been observed [17,21], and the effects of electron loss in LHCD plasmas have also been seen [19]. ICRF-only heated discharges provide the opportunity for the study of toroidal rotation in plasmas with no direct momentum input. Co-current rotation in ICRF-only plasmas [31,32,33] has been documented; the JET results were alternately explained by high energy ion loss [31] and the effects of the ion pressure gradient [32].

The main Alcator C-Mod results [33] are summarized here: during the ICRF pulse, and in the absence of direct momentum input, the rotation is in the co-current direction (opposite to that during the ohmic portion of the discharge). When the plasma current direction is reversed, the rotation during ICRF heating also switches, remaining in the co-current direction. The magnitude of the rotation is largest ($\sim$1.3 $\times$ 10^5 m/s, 200 kRad/s) during the best H-mode discharges. The magnitude of the rotation velocity during ICRF heating increases with the stored energy increase, insensitive to the input power or electron density, over a range of two orders of magnitude. The plasmas with the highest H-factors rotate the fastest. In general, the rotation is not an effect only of H-mode *per se*, in that some high H-factor L-mode plasmas rotate faster than some modest H-factor H-mode plasmas. However, in some discharges with similar target parameters and the same ICRF power, only those plasmas which enter H-mode exhibit substantial rotation. In addition, purely ohmic H-Mode plasmas also rotate in the co-current direction. The toroidal rotation velocity in ICRF heated ELM-free H-mode discharges is peaked at the magnetic axis, and falls off quickly with minor radius. Any poloidal component of the impurity rotation velocity inside of r/a = 0.3 is $\leq$ 3 $\times$ 10^3 m/s. Values of E_r up to 30 kV/m at r/a = 0.3 have been inferred, although $V_P B_T/B_P$ has been ignored compared to V_T. The rotation velocity decays with a characteristic time between 50 and 100 ms after the ICRF is turned off, comparable to the energy confinement time, and much shorter than the predicted neoclassical momentum slowing down time.

The theoretical approach to impurity rotation in ICRF heated plasmas has been from two directions. The standard neo-classical treatment of rotation [34-36] has been expanded to include impurity species properly [28]; however the electric field was not calculated. Recently, the radial electric field and plasma rotation have been calculated [37] at the plasma edge in the region of the transport barrier from a nondegenerate ambipolarity constraint obtained by extending the neo-classical theory to small scale lengths. The effects of ion orbit loss have been shown to give rise to poloidal rotation [38] and radial ion transport induced by ICRF waves [39,40] has been calculated. The direct momentum absorption of ICRF waves by ions has been calculated for JET plasmas [32], and is found to be small, in the counter-current direction and therefore not an important factor in spawning the observed rotation. ICRF waves can drive non-ambipolar radial transport, generating an E_r

and plasma rotation, through shifts of resonant ion orbits[41]. Toroidal rotation generated by toroidally directed ICRF waves has been calculated [42] and toroidal rotation associated with a special class of magnetosonic-whistler modes excited by ICRF waves has also been considered [43].

In this paper, recent results of impurity toroidal rotation measurements in ICRF heated Alcator C-Mod plasmas are presented. The experimental setup is described, the correlation between the velocity increase and the plasma stored energy increase (confinement improvement) is demonstrated and the increase in the rotation velocity with decreasing plasma current is shown in Section II. Scalings of the toroidal rotation velocity in D(H) ICRF heated plasmas with the H/D ratio and the resonance location are also shown in Section II, along with results from D(^{3}He) heating at 8 T and ohmic H-modes. Comparisons of observed rotation velocity profiles with those calculated from neo-classical theory are made in Section III, and the effects of ICRF induced ion orbit shifts on the toroidal rotation are considered in Section IV. Conclusions are drawn in Section V.

II. Experiment Description, Observations of Toroidal Rotation and Scaling with Plasma Current

The observations presented here were obtained from the Alcator C-Mod [44] tokamak, a compact (major radius R = 0.67 m, typical minor radius of 0.22 m, and elongation $\kappa \leq 1.8$), high field device ($2.6 \leq B_T \leq 7.9$ T) in the lower single null configuration, which has operated with plasma currents between 0.23 and 1.5 MA and volume averaged electron densities between 0.24 and 5.9 $\times 10^{20}/m^3$. Up to 4 MW of ICRF power at 80 MHz [45] are available, from 2 dipole antennas, each with $0 - \pi$ phasing; most of the cases described here are with H minority heating in deuterium plasmas at 5.4 T. Central electron and ion temperatures are in the range from 2 to 5 keV. During normal operation, the plasma current is in the clockwise direction as viewed from the top of the machine. X-ray spectra are recorded with a spatially fixed von Hamos type crystal x-ray spectrometer [46], whose line of sight is tangent to the plasma axis, pointing in the counter clockwise direction, as seen from above. Rotation velocities have been determined from the Doppler shifts of the Ar^{17+} Lyman α doublet [47,48] (1s $^1S_{\frac{1}{2}}$ - 2p $^2P_{\frac{3}{2}}$ at 3731.10 mÅ, and 1s $^1S_{\frac{1}{2}}$ - 2p $^2P_{\frac{1}{2}}$ at 3736.52 mÅ). For the central temperature range of Alcator C-Mod, hydrogenlike argon is a central charge state. Spectra are typically collected every 20 ms during plasma discharges. Argon is routinely injected into Alcator C-Mod plasmas through a piezoelectric valve, to provide x-ray transitions for Doppler width ion temperature measurements. Absolute wavelength calibration was obtained from the potassium K_α lines generated from a KCl fluorescence x-ray source [48].

During ICRF heating with the normal current direction, the spectra are blue-shifted, indicating impurity rotation in the co-current direction. The central argon rotation velocity has been determined under a wide range of plasma conditions and scalings with plasma parameters have been identified. The strongest correlation that has emerged from a parameter scaling study is the relationship with the plasma stored energy; there is a general increase in the toroidal rotation velocity with increasing stored energy [33]. Shown in Fig.1 is the increase in the impurity toroidal rotation velocity as a function of the increase in the plasma stored energy during the ICRF injection, for a large number of H- and L-mode plasmas. Generally speaking, the points fall into two groups; for stored energy increases above 20 kJ, the plasmas are mostly in H-mode, while for increases below 20 kJ, the plasmas are in L-mode, mainly because the total power is below the H-mode threshold. There are, however, several L-mode points with stored energy increases around 50 kJ; these are from reverse current discharges or plasmas with high magnetic field, which did not exhibit the characteristic drop in the D_α emission and edge pedestal formation, and therefore are not considered H-mode, although in some cases the H-factors (ITER 89-P) were as large as 1.5. This data set includes a range of RF powers between 0.5 and 3.6 MW, central electron densities between 0.9 and 5.9 $\times 10^{20}/m^3$, toroidal magnetic fields between 5 and 8 T, plasma currents between

0.6 and 1.2 MA, and with normal (clockwise) and reverse currents, in both L- and H-mode plasmas, with H-factors between 0.75 and 2.3. There are also some ohmic H-mode discharges, shown as triangles, comparing the pre-H-mode to H-mode portions, which exhibit the same dependence of rotation velocity increasing with stored energy.

While the trend of increasing rotation velocity with increasing stored energy is clear, there is a certain amount of scatter in the data, which may be largely due to effects of the plasma current. In otherwise similar plasmas with comparable stored energy increases, the toroidal rotation is higher in plasmas with lower current. This effect is demonstrated in Fig.2, where the time histories of the plasma current, stored energy and rotation velocity are shown for two D(H) discharges at 5.4 T with 2.5 MW of ICRF power between 0.6 and 1.2 s. The stored energy increase during the ICRF pulse in both cases is about 45 kJ, although the 1 MA plasma has a higher stored energy target plasma before 0.6 s. The 600 kA plasma rotates about a factor of two faster compared to the higher current case. Another perspective on this effect is illustrated in Fig.3. In the top of the figure are the trajectories in the Stored Energy - Rotation Velocity plane of the two discharges of Fig.2, in addition to two other similar discharges each at 0.6 and 1.0 MA. Both sets of plasmas begin at the same velocity, and reach the same velocity throughout the ICRF pulse, around 4×10^4 m/s, whereas the peak stored energy in the higher current plasmas is almost twice as large. In the bottom of the figure are the same trajectories, with the stored energy normalized to the plasma current, which brings the two sets of discharges on top of each other. Scaling of the rotation velocity with β_P instead of W_P/I_P is not as good since an ${I_P}^{-2}$ dependence is too strong. This trend of higher rotation with lower plasma current is emphasized in Fig.4, which is a linear plot of the 5.4 T, H-mode points from Fig.1, sorted by plasma current. While most of the discharges in this data base are with 0.8 and 1.0 MA of plasma current, it's clear that those shots with higher current rotate slower than those with lower current, for the same stored energy increase. A vertical slice of this figure between 40 and 60 kJ is shown in Fig.5, again emphasizing this trend; the rotation velocity decreases substantially with increasing plasma current for a fixed stored energy increase. Sorting the points of Fig.1 by electron density in a similar fashion as in Fig.4 does not reveal any obvious dependence on n_e. Although there is a general tendency for discharges with higher ICRF power to have higher stored energy and faster rotation, there can be factors of three variation in these quantities at fixed launched ICRF power for similar target plasma current and density. Perhaps this is caused by differences in the absorbed power, which may in part be due to variations in the hydrogen minority fraction, or to other variables such as edge plasma shaping and wall conditioning.

For D(H) heating at 5.4 T, the increase of the stored energy and rotation velocity during the ICRF pulse is observed to be a strong function of the hydrogen to deuterium ratio in the plasma. Because of the trade-off between ICRF wave absorption and the minority tail formation, the optimum H/D ratio is calculated to be in the vicinity of 5% [49]. Shown in Fig.6 are the stored energy and rotation velocity increases as a function of the H/D ratio during the ICRF pulse for a sequence of 0.8 MA plasmas with target densities between 1.5 and 1.8 $\times$ $10^{20}/m^3$. Two sets of discharges are shown, from a range of RF powers between 2 and 2.5 MW, and between 1 and 1.5 MW. The H/D ratio was determined from the Balmer H_α to D_α brightness ratio at the plasma edge, and is taken to be the same as at the plasma center. The maximum stored energy and rotation velocity increases are with H/D ratios between 5 and 10 %. The H/D ratio in this figure was scanned passively over a three week period during normal wall conditioning, including boronization.

By varying the toroidal magnetic field, the ICRF wave resonance location may be shifted to larger minor radius, and the heating efficiency is expected to drop [50]. In an extreme case with the resonance located near the plasma edge, the ICRF should have little or no effect on the plasma. Shown in Fig.7 are several parameter time histories for a 6.9 T, 1.0 MA, D(H) discharge (H/D $\sim$ 5%) with the resonance location at R=0.87 m (r/a = 0.9). In this L-mode case there was no measurable rotation, a slight stored energy increase of 10-15 kJ and very little temperature increase, although the ICRF power was 2.6 MW. The results of the complete resonance location scan are shown in Fig.8, where the central rotation velocity and stored energy are displayed; both fall off rapidly when the resonance is located near the edge. For this scan the resonance location was varied by adjusting the toroidal magnetic field from 5.5 to 6.9 T, while raising the plasma current from 0.84 to 1.01 MA, maintaining $q_{\psi_{95}} = 4.7$. It is not clear whether this drop in the central rotation is an effect of directly moving the resonance location, from simply the associated fall in the plasma stored energy, or a decline in the absorbed power.

Most of the points included in Fig.1 were obtained from D(H) plasmas with toroidal magnetic fields near 5.4 T and with H/D ratios between 5 and 10%. There are several D(^{3}He) discharges at 7.9 T which exhibit similar rotation characteristics. Shown in Fig.9 are comparisons of several parameter time histories for a D(H) and a D(^{3}He) discharge. The stored energy increase in both cases was around 55 kJ during the ICRF pulse, and the rotation velocities are also similar. In these two cases the minority fraction was about 4%, but the electron densities and electron and ion temperatures were somewhat different. The 7.9 T discharge had $q_{\psi_{95}} = 4.7$ and RF power of 3.0 MW, while the 5.4 T discharge had $q_{\psi_{95}} = 3.6$ and RF power of 2.5 MW. Both of these differences would make for slightly slower rotation in the 5.4 T case. However, the main point is that the toroidal rotation is *similar* in D(^{3}He) discharges at 7.9 T and D(H) discharges at 5.4 T, in spite of the fact that D(^{3}He) minority heating requires multi-pass absorption at these minority concentrations. It should also be mentioned that not all of the 7.9 T discharges exhibit H-mode characteristics.

The rotation velocity during ICRF heating does not seem to be a strong function of the impurity mass. The occurence of a Mo^{32+} line ($2p^6$ - $(2p^5)_{\frac{3}{2}}4d_{\frac{5}{2}}$ at 3739.8 mÅ[51]) in the same spectrum with the Ar^{17+} doublet allows a comparison of the rotation velocities of impurities with substantially different masses to be made. Shown in Fig.10 are the rotation velocity times histories for molybdenum (100 AMU) and argon (40 AMU) from a 0.85 MA, 5.7 T, D(H) discharge. The rotation velocities of these two ions are very similar during the 2.7 MW ICRF pulse, indicating that impurity diamagnetic effects are unimportant for low impurity densities. (Note the delay between the rises and falls of the rotation signals relative to the ICRF waveform). The charge to mass ratio for these two ions are .32 for Mo and .42 for Ar. Argon and molybdenum rotation velocities are also the same during ohmic discharges [27].

It remains an open question whether the ICRF induces the rotation, or the rotation is simply a consequence of the stored energy increase and the association between momentum and energy confinement. Shown in Fig.11 are several time histories from two 1.0 MA, 5.4 T D(H) discharges which had very similar core target plasma parameters, one of which entered H-mode while the other remained in L-mode. The H-mode plasma had a substantial stored energy increase and fast rotation, with the same launched ICRF power (2.5 MW) as the L-mode plasma. Both plasmas were close to the H-mode threshold before the ICRF pulse, and there were *subtle* differences in the target plasmas; the H-mode plasma had an average triangularity of 0.5 and a divertor pressure of 13 mTorr before the ICRF, while the L-mode plasma had δ=0.41 and a divertor pressure of 42 mTorr. It is most likely that the high divertor pressure in the L-mode case prevented the edge electron temperature from rising above the H-mode threshold [52]. How this, and the different triangularities affected the coupling and absorption of ICRF power is unknown. There was however a significant increase in the central ion temperature in the L-mode case. In spite of the 2.5 MW of ICRF power in the L-mode case, neither the stored energy nor rotation velocity responded significantly.

The issue of whether the rotation is a consequence of the stored energy increase or is generated directly by the ICRF waves may be addressed by operating ohmic H-mode plasmas. During ohmic H-modes, the plasmas also rotate in the co-current direction, changing direction from the counter-current observed rotation during the ohmic L-mode phase. The scaling of the rotation velocity with the stored energy during the H-mode is very similar to that seen in ICRF heated plasmas, as shown in Fig.1, although the velocities and stored energies in these discharges are quite modest when compared to the best ICRF H-mode cases. These Ohmic H-modes were achieved by operating at 4.0 T with 1.0 MA of current, and Ohmic input powers around 2 MW.

III. Comparison with Neo-Classical Theory

In an effort to understand this rotation from basic neo-classical considerations, the discharge shown in Fig.12 has been analyzed, both before and during the ICRF injection. Prior to the ICRF pulse, this 1.0 MA, 5.7 T D(H) discharge had a central electron density of $2.3 \times 10^{20}/\mathrm{m}^3$ and was rotating at about 1×10^4 m/s in the counter current direction. Well into the H-mode after 1 second with 3.2 MW of ICRF power, the electron density rose to $4.4 \times 10^{20}/\mathrm{m}^3$ and the central argon toroidal rotation velocity increased to 1×10^5 m/s in the co-current direction. While the time histories of the stored energy and the toroidal rotation are very similar, there is a slight delay in the rotation (for example in the dip around 0.85 s), which indicates that the central rotation is an effect of the improved confinement rather than the cause. The rise time of the central rotation (and decay time) is typically 50-100 ms [33], similar to the energy confinement time in H-mode [53]. Throughout this discharge, the impurity strength parameter α, defined as $n_I\ Z_I{}^2/n_i\ Z_i{}^2$ (where I denotes impurity and i denotes majority ion), is less than 0.007.

Theoretical expressions for the neo-classical impurity and majority ion toroidal and poloidal rotation velocities are given by Eqns.(37), (38), (33) and (34), respectively, of Ref.[28]. These expressions are obtained by solving the parallel momentum and heat flow balance equations, including one impurity species. No effects of ion orbit shifts have been included, nor have the individual charge states for the impurity species. These rotation velocities may be written (in the absence of a parallel electric field) as

$$V_T^I = \frac{1}{B_P}\left[E_r + \frac{(K_1 + \frac{3}{2}K_2 - 1)}{e}\frac{\partial T_i}{\partial r} - \frac{T_i}{en_i}\frac{\partial n_i}{\partial r}\right] \quad (1),$$

$$V_T^i = \frac{1}{B_P}\left[E_r + \frac{(K_1 - 1)}{e}\frac{\partial T_i}{\partial r} - \frac{T_i}{en_i}\frac{\partial n_i}{\partial r}\right] \quad (2),$$

$$V_P^I = \frac{1}{B_T}\left[\frac{(K_1 + \frac{3}{2}K_2 - 1)}{e}\frac{\partial T_i}{\partial r} - \frac{T_i}{en_i}\frac{\partial n_i}{\partial r} + \frac{T_I}{Z_I en_I}\frac{\partial n_I}{\partial r}\right] \quad (3)$$

and

$$V_P^i = \frac{1}{B_T}\frac{K_1}{e}\frac{\partial T_i}{\partial r} \quad (4).$$

Here the subscripts T and P denote toroidal and poloidal, e is the electric charge, B is the magnetic field, T and n are the temperature and density, K_1 and K_2 are functions of the viscosity matrix elements, inverse aspect ratio and the impurity strength parameter (evaluated for all collisionality regimes in the appendix of Ref.[28]) and E_r is the radial electric field. Note that the V_Ps are independent of E_r. Eqn.(1) (and Eqns.(2-4)) is very weakly dependent on the impurity species in Alcator C-Mod plasmas; for low values of α, the expressions for K_1 and K_2 are insensitive to the impurity mass. This agrees with the observations of Fig.10, that the rotation velocities measured for argon and molybdenum are the same, within the measured uncertainties.

The rotation velocities in Eqns.(1-4) have been evaluated from the observed electron temperature profiles (the ion temperature profiles are taken to be the same for this high density plasma) [54], the measured electron density profiles (the ion density profiles are taken to be the same for this low Z_{eff} plasma) [55], the measured argon density and temperature (from the intensities and widths of the Ar^{16+} lines [56]) and the magnetic field and q profiles calculated from the magnetics diagnostic using the EFIT magnetics code [57]. The only quantity not directly measured in

Eqns.(1-4) is E_r. Regardless of the origin of E_r, or its particular magnitude, V_T is inversely proportional to B_P, which agrees *qualitatively* with the I_P scaling shown in Figs.3 and 5. Shown in Fig.13 are the theoretical argon toroidal rotation velocity profiles for the discharge of Fig.12 evaluated at 0.4 seconds, before the ICRF pulse, and at 1.3 seconds, well into the ICRF H-mode. E_r has been set to zero in the calculations since there is no independent or direct measurement. The theoretical velocities are small everywhere except near the plasma edge, where the ion density and temperature gradients are largest. ($E_{||}$ has not been included in these calculations, which would induce negative central rotation in the ohmic L-mode case, see Refs.[27,28].) The measured central argon toroidal rotation velocities are shown by the symbols; the ohmic point is close to the calculated value with E_r=0. In the ICRF H-mode case the calculated rotation velocity near the edge has increased by a factor of 2-3, and the peak has narrowed, because of the formation of the edge 'pedestal' [52,53], a steepening of the edge temperature and density gradients. Currently there is no direct measurement of the edge toroidal rotation on Alcator C-Mod for comparison. Near the plasma center there is little difference in the calculated argon toroidal rotation velocity with E_r set to zero for the two different times during this discharge, whereas there is a large difference in the measured values. This indicates that it is *not* the onset of the steep edge ion pressure gradient which directly causes the central impurity toroidal rotation, and the presence of a substantial core E_r is implied during the ICRF heating.

More complete measured central impurity rotation profiles [33] for an ELM-free ICRF H-mode plasma, along with the calculations (E_r is again not included in the toroidal velocities) are shown in Fig.14. Also shown are the calculated *deuteron* rotation velocity profiles. The argon (impurity) and deuteron (ion) poloidal rotation velocities near the edge are not expected to be the same, and this has been observed in DIII-D [22]. The measured core value for the argon poloidal rotation velocity is $0 \pm 3 \times 10^3$ m/s [33], consistent with the calculations. (This justifies ignoring $V_P B_T / B_P$ compared to V_T.) However, the central impurity toroidal rotation profiles can only be made to agree with the calculations by inclusion of a substantial core E_r. The suggestion is that during the ICRF H-mode, there is the formation of a strong radial electric field [33] near the plasma center which possibly drives the central toroidal rotation. Whether E_r is caused directly by the ICRF waves, or arises from another mechanism associated with the plasma stored energy increase is not known.

IV. Comparison with Ion Orbit Shift Model

One possible mechanism that can give rise to E_r is an inward shift of energetic ion orbits induced by ICRF waves [41,58,59]. The key features of this mechanism are summarized here. For Alcator C-Mod conditions, the shift of ions is inward, and the resulting toroidal rotation from the large $E_r > 0$ will always be in the co-current direction [58]. This agrees with the Alcator C-Mod observations of co-current toroidal rotation, which switches direction when the plasma current direction is reversed, remaining co-current [33]. The magnitude of the calculated V_T is roughly consistent with the observed values, if it is assumed that the toroidal momentum confinement time is the same as the energy confinement time [59] (which is observed in Alcator C-Mod). The Doppler shifted symmetry breaking effects from on-axis heating get weaker at larger minor radius because the relative amount of Doppler shift, compared to the orbital minor radius, becomes smaller at larger minor radius. Thus on-axis heating should yield localized E_r, toward the plasma center, which agrees qualitatively with the observations of Fig.14 and Ref.[33], and with the resonance location scan shown in Fig.8. The origin of the radial current j_r^{rf} is the increase of the radial orbit shift as the perpendicular energy is increased. Since the radial orbit shift is inversely proportional to the plasma current, the driven E_r should also be inversely proportional to the plasma current. This is consistent with the decrease in the central toroidal rotation velocity with increasing plasma current shown in Fig.5. By changing the H/D ratio, by which the minority tail energy can be varied, so the Doppler shifted resonance location is no longer favorable, the rotation should be reduced, which agrees with the results of Fig.6. Furthermore, by varying the antenna phasing to $0 - \pi/2$, it should be possible to generate even stronger rotation, and associated improved energy confinement, but this has not yet been tested.

Many of the same features of the rotation predicted by this ion orbit shift model would be expected for plasma heating or stored energy increases, such as the scalings with H/D ratio or resonance location. Whether the rotation is directly generated by the ICRF waves or is simply tied (by some unknown mechanism) to the stored energy increase caused by the ICRF has not been determined. The ion orbit shift model predicts the observed scaling with plasma current, but that is also consistent with the basic neo-classical theory. If the rotation were only a consequence of being in H-mode, then the co-current direction must be explained, in addition to the strong observed rotation in some L-mode plasmas.

V. Conclusions

Strong co-current toroidal impurity rotation has been observed in the center of Alcator C-Mod ICRF heated discharges. The magnitude of the rotation increases with increasing plasma stored energy, and decreases with increasing plasma current. The rotation is independent of impurity mass, and is insensitive to electron density, ICRF power and minority species (H vs ^{3}He) in deuterium plasmas. In D(H) heated plasmas, the maximum rotation is observed with an H/D ratio between 5 and 10 %, and with the resonance location in the inner half of the plasma. Significant rotation is also observed in D(^{3}He) discharges at 7.9 T, and co-current rotation is seen during ohmic H-modes. Comparisons with neo-classical theory, (which predict a $1/B_P$ dependence and impurity mass independence, and show consistency with certain observed features of the rotation) indicate that the ion pressure gradient is an unimportant contributor to the central impurity rotation and the presence of a substantial core radial electric field is inferred during the ICRF pulse. A radially inward shift of resonant tail minority ions could generate this E_r. For Alcator C-Mod parameters, this could give rise to toroidal rotation in the co-current direction, with a magnitude similar to the observed rotation. From a comparison of H- and

L-mode plasmas, it's clear that the rotation is intimately tied to stored energy, regardless of its origin.

VI. Acknowledgements

The authors thank M. Porkolab and C. K. Phillips for useful discussions, J. Harker for computational assistance, J. Terry for D_α measurements, J. Irby for electron density measurements, A. Hubbard for electron temperature measurements, C. Fiore for ion temperature measurements, R. Granetz for magnetics measurements, T. Tutt for H_α to D_α brightness measurements, J. Ke for assistance with the neoclassical calculations and the Alcator C-Mod operations and RF groups for expert running of the tokamak. Work supported at MIT by DoE Contract No. DE-FC02-99ER54512.

References

[1] K.C.Shiang and E.C.Crume, Phys. Rev. Lett. **63** (1989) 2369.

[2] K.H.Burrell et al., in *Plasma Physics and Controlled Nuclear Fusion Research 1994* Proceedings of the 15th International Conference, Seville, Spain, Vol.1 (IAEA, Vienna 1996) 221.

[3] P.H.Diamond et al., in *Plasma Physics and Controlled Nuclear Fusion Research 1994* Proceedings of the 15th International Conference, Seville, Spain, Vol.3 (IAEA, Vienna 1996) 323.

[4] R.A. Moyer et al., Phys. Plasmas **2** (1995) 2397.

[5] R.J.Groebner et al., Phys. Rev. Lett. **64** (1990) 3015.

[6] F.Wagner et al., in *Plasma Physics and Controlled Nuclear Fusion Research 1990* Proceedings of the 13th International Conference, Wahington D.C., Vol.1 (IAEA, Vienna 1991) 277.

[7] Y.Miura et al., in *Plasma Physics and Controlled Nuclear Fusion Research 1990* Proceedings of the 13th International Conference, Wahington D.C., Vol.1 (IAEA, Vienna 1991) 325.

[8] S.Suckewer et al., Nucl. Fusion **21** (1981) 1301.

[9] K.H.Burrell et al., Nucl. Fusion **28** (1988) 3.

[10] A.Kallenbach et al., Plasma Phys. Contr. Fusion **33** (1991) 595.

[11] N.Asakura et al., Nucl. Fusion **33** (1993) 1165.

[12] M. Mattioli et al., J. Appl. Phys. **64** (1988) 3345.

[13] R.Bartiromo et al., Rev. Sci. Instrum. **60** (1989) 237.

[14] H.Weisen et al., Nucl. Fusion **29** (1989) 2187.

[15] W.A.Peebles et al., in *Plasma Physics and Controlled Nuclear Fusion Research 1990* Proceedings of the 13th International Conference, Washington D.C., Vol.1 (IAEA, Vienna 1991) 589.

[16] S.D.Scott et al., Phys. Rev. Lett **64** (1990) 531.

[17] K. Ida et al., Nucl. Fusion **31** (1991) 943.

[18] B.P. Duval, B. Joye and B. Marchal, Nucl. Fusion **32** (1992) 1405.

[19] Y.Koide et al., in *Plasma Physics and Controlled Nuclear Fusion Research 1992* Proceedings of the 14th International Conference, Wurzburg, Vol.1 (IAEA, Vienna 1993) 777.

[20] K. Nagashima et al., Nucl. Fusion **34** (1994) 449.

[21] H.Hsuan et al., in *Proceedings of the 11th Topical Conference on Radio-Frequency Power in Plasmas*, Palm Springs, CA 1995, AIP Conference Proceedings 355 (Editors: Ronald Prater, Vincent S. Chan) American Institute of Physics, Woodbury, New York 1996 p. 39

[22] J. Kim et al., Phys. Rev. Lett. **72** (1994) 2199.

[23] R.E.Bell et al., Plasma Phys. Contr. Fusion **40** (1998) 609.

[24] Y. Miura et al., Plasma Phys. Contr. Fusion **40** (1998) 799.

[25] P. Gohil et al., Nucl. Fusion **38** (1998) 93.

[26] K. Ida, Plasma Phys. Contr. Fusion **40** (1998) 1429.

[27] J.E.Rice et al., Nucl. Fusion **37** (1997) 421.

[28] Y.B.Kim, P.H.Diamond and R.J.Groebner, Phys. Fluids B **3** (1991) 2050.

[29] S.Yamamoto et al., in *Plasma Physics and Controlled Nuclear Fusion Research 1982* Proceedings of the 9th International Conference, Baltimore, Vol.1 (IAEA, Vienna 1983) 73.

[30] V.I.Bugaraya et al., Nucl. Fusion **25** (1985) 1707.

[31] L.-G.Eriksson et al., Plasma Phys. Contr. Fusion **34** (1992) 863.

[32] L.-G.Eriksson et al., Plasma Phys. Contr. Fusion **39** (1997) 27.

[33] J. E. Rice et al., Nucl. Fusion **38** (1998) 75.

[34] F.L.Hinton and R.D.Hazeltine, Rev. Mod. Phys. **48** (1976) 239.

[35] S.P.Hirshman and D.J.Sigmar, Nucl. Fusion **21** (1981) 1079.

[36] F.L.Hinton, Phys. Fluids B **3** (1991) 696.

[37] A.L.Rogister, Phys. Plasmas **6** (1999) 200.

[38] K.C.Shaing, Phys. Fluids B **4** (1992) 171.

[39] L. Chen et al., Nucl. Fusion **28** (1988) 389.

[40] C.S.Chang et al., Phys. Fluids B **3** (1991) 3429.

[41] C.S.Chang et al., 1998 International Sherwood Fusion Theory Conference, Oral Paper 2B1 (March 23 - 25, 1998, Atlanta, Georgia)

[42] T. Hellsten et al., in *Plasma Physics and Controlled Nuclear Fusion Research 1998* Proceedings of the 17th International Conference, Yokohama, IAEA-F1-CN-69/THP2/36.

[43] B. Coppi et al., in *Plasma Physics and Controlled Nuclear Fusion Research 1998* Proceedings of the 17th International Conference, Yokohama, IAEA-F1-CN-69/TH3/7.

[44] I.H.Hutchinson et al., Phys. Plasmas **1** (1994) 1511.

[45] S.N.Golovato, M. Porkolab, Y. Takase et al., in *Proceedings of the 11th Topical Conference on Radio-Frequency Power in Plasmas*, Palm Springs, CA 1995, AIP Conference Proceedings 355 (Editors: Ronald Prater, Vincent S. Chan) American Institute of Physics, Woodbury, New York 1996 p.23

[46] E.Källne, J.Källne, E.S.Marmar and J.E.Rice, Phys. Scr. **31** (1985) 551.

[47] G. W. Erickson, J. Phys. Chem. Ref. Data **6** (1977) 831.

[48] E.S.Marmar et al., Phys. Rev. A **33** (1986) 774.

[49] M. Porkolab et al., in *Advances in Plasma Physics* AIP Conf. Proceedings 314 (AIP, NY, 1994, Editor: N. S. Fisch) p. 99.

[50] Y.Takase et al., in *Proceedings of the Twelfth Topical Conference on Radio Frequency Power in Plasmas* (Savannah, GA, 1997), AIP Conf. Proceedings 403 (AIP, NY, 1997, Editors: P. M. Ryan and T. Intrator) p. 33.

[51] J.E.Rice et al., Phys. Rev. A **51** (1995) 3551.

[52] A. E. Hubbard et al., Plasma Phys. Contr. Fusion **40** (1998) 689.

[53] M. Greenwald et al., Nucl. Fusion **37** (1997) 793.

[54] T.C.Hsu et al., Proc. 8th Joint Workshop on ECE and ECRH, IPP III/186 (1993) 409.

[55] J.H.Irby et al., Rev. Sci. Instrum. **59** (1988) 1568.

[56] J. E. Rice et al., Fusion Eng. Des. **34** and **35** (1997) 159.

[57] L. L. Lao et al., Nucl. Fusion **25** (1985) 1611.

[58] C.S. Chang et al., in *Plasma Physics and Controlled Nuclear Fusion Research*

1998 Proceedings of the 17th International Conference, Yokohama, IAEA-F1-CN-69/THP2/34.

[59] C.S. Chang et al., to appear in Phys. Plasmas (1999).

Figure Captions

Fig. 1 The toroidal rotation velocity increases during the ICRF pulse as a function of the plasma stored energy increases in H-mode (L-mode) discharges are shown as asterisks (circles). Ohmic H-mode discharges are shown as triangles.

Fig. 2 The time histories of the plasma current and ICRF pulse (top frame), plasma stored energy (middle frame) and argon toroidal rotation velocity (bottom frame) for a 0.6 MA discharge (solid line) and a 1.0 MA discharge (dash-dot-dot-dot line).

Fig. 3 Trajectories in the W_P-V_{Tor} plane during ICRF heated discharges at 0.6 MA (solid) and 1.0 MA (dash-dot-dot-dot) plasma current (top), and the same trajectories with W_P normalized by I_P (bottom).

Fig. 4 The toroidal rotation velocity increase during the ICRF pulse as a function of the plasma stored energy increase, sorted by plasma current. Triangles- 0.6 MA, asterisks- 0.8 MA, diamonds- 1.0 MA and $\times$s- 1.2 MA. The 0.8 and 1.0 MA points have been averaged within 1.5 and 2.5 kJ bins, respectively. The solid curves are best linear fits for the three highest current points.

Fig. 5 The toroidal rotation velocity as a function of plasma current for stored energy increases between 40 and 60 kJ. The 1.5 MA point is from a single discharge.

Fig. 6 The stored energy (top) and toroidal rotation velocity (bottom) increases during the ICRF pulse as a function of the hydrogen to deuterium ratio, for 0.8 MA target plasmas, with central electron densities between 1.5 and 1.8 $\times$ 10^{20}/m^3.

Fig. 7 Parameter time histories for a 6.9 T, 1.0 MA, D(H) discharge with the resonance location at 19.8 cm (r/a = 0.9). In the top frame is the plasma stored energy. In the second frame are the central electron density (solid) and the central argon density (dash-dot-dot-dot, $\times 10^4$). In the third frame are the central electron temperature (with sawteeth) and the central ion temperature (smooth). In the fourth frame is the ICRF power and in the fifth frame is the D_α emission. In the bottom frame is the central toroidal rotation velocity of argon ions.

Fig. 8 The central toroidal rotation velocity (triangles) and plasma stored energy (asterisks) as a function of resonance location, for a series of discharges similar to that shown in Fig.7.

Fig. 9 The time histories of several parameters for a 5.4 T, 1.0 MA D(H) discharge (dash-dot-dot-dot) and a 7.9 T, 1.2 MA D(^{3}He) discharge (solid). In the top frame are the plasma stored energies. In the second frame are the central electron densities and in the third frame are the central ion temperatures. In the fourth frame are the ICRF power pulses and in the fifth frame are the toroidal magnetic field waveforms. In the bottom frame are the central toroidal rotation velocities of argon ions.

Fig. 10 The time histories of the argon (solid) and molybdenum (dash-dot-dot-dot) toroidal rotation velocites for a 0.85 MA, 5.7 T hydrogen minority discharge. Also shown is the 2.7 MW ICRF pulse.

Fig. 11 A comparison of parameter time histories for an H- (solid) and L-mode (dash-dot-dot-dot) plasma. The legend is the same as Fig.9 except in the fifth frame are shown the D_α waveforms.

Fig. 12 The time histories of several parameters for a 5.7 T, 1.0 MA deuterium H-mode discharge. The legend is the same as in Fig.12.

Fig. 13 Calculated toroidal rotation velocity profiles for argon ions for the discharge of Fig.7 with the measured parameters evaluated at 0.4 seconds (dash-dot-dot-dot) and 1.3 seconds (solid). The diamond (asterisk) shows the measured argon toroidal rotation velocity at 0.4 (1.3) seconds.

Fig. 14 Calculated toroidal (top frame) rotation velocity profiles for argon ions (solid) and deuterons (dash-dot-dot-dot) and poloidal rotation velocity profiles (bottom frame) for an ELM-free ICRF H-mode discharge. The asterisks show the measured argon toroidal and poloidal rotation velocities, with error bars.

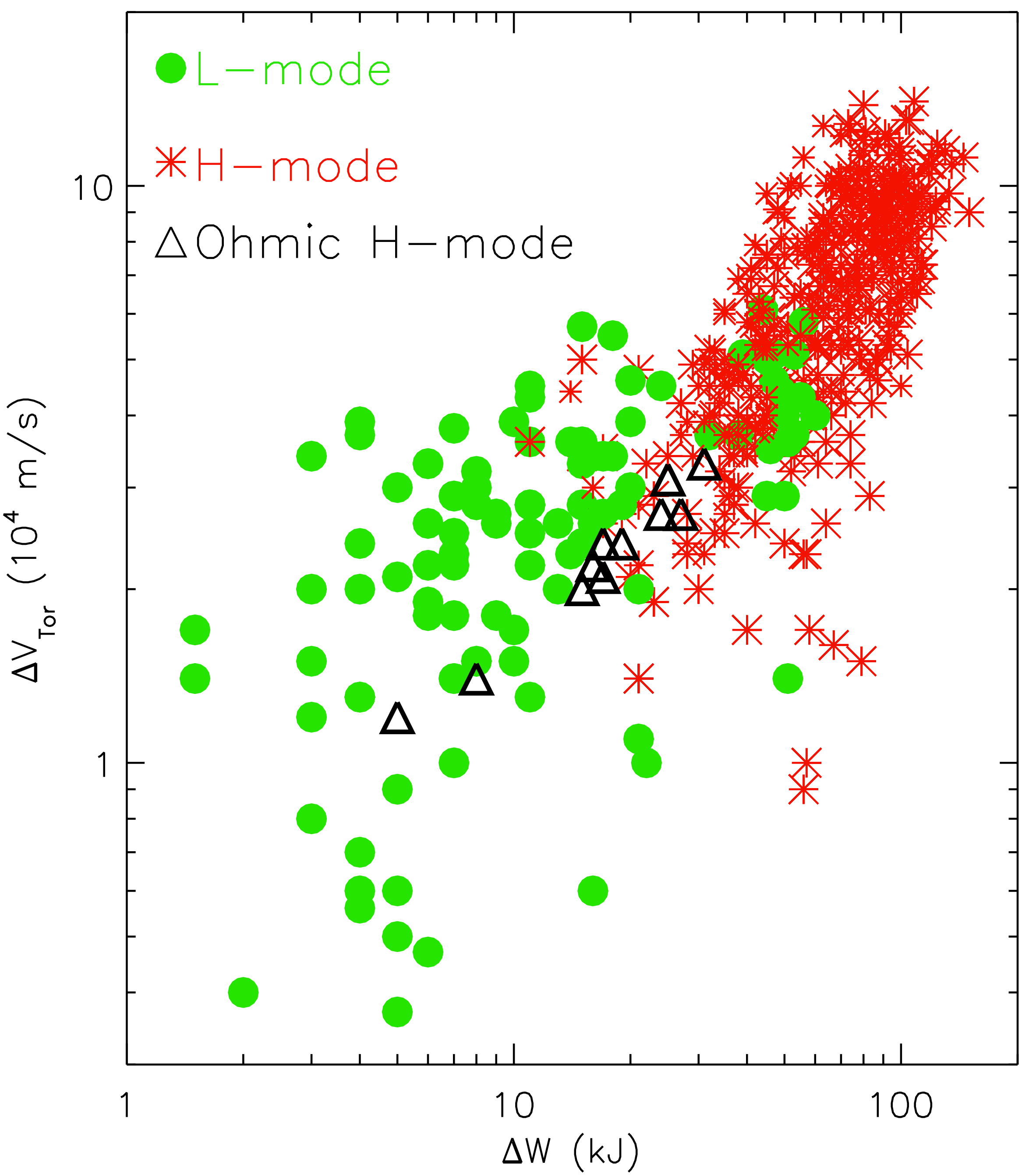

L−mode
H−mode
Ohmic H−mode
10
1
1
10
100
ΔV_Tor (10^4 m/s)
ΔW (kJ)

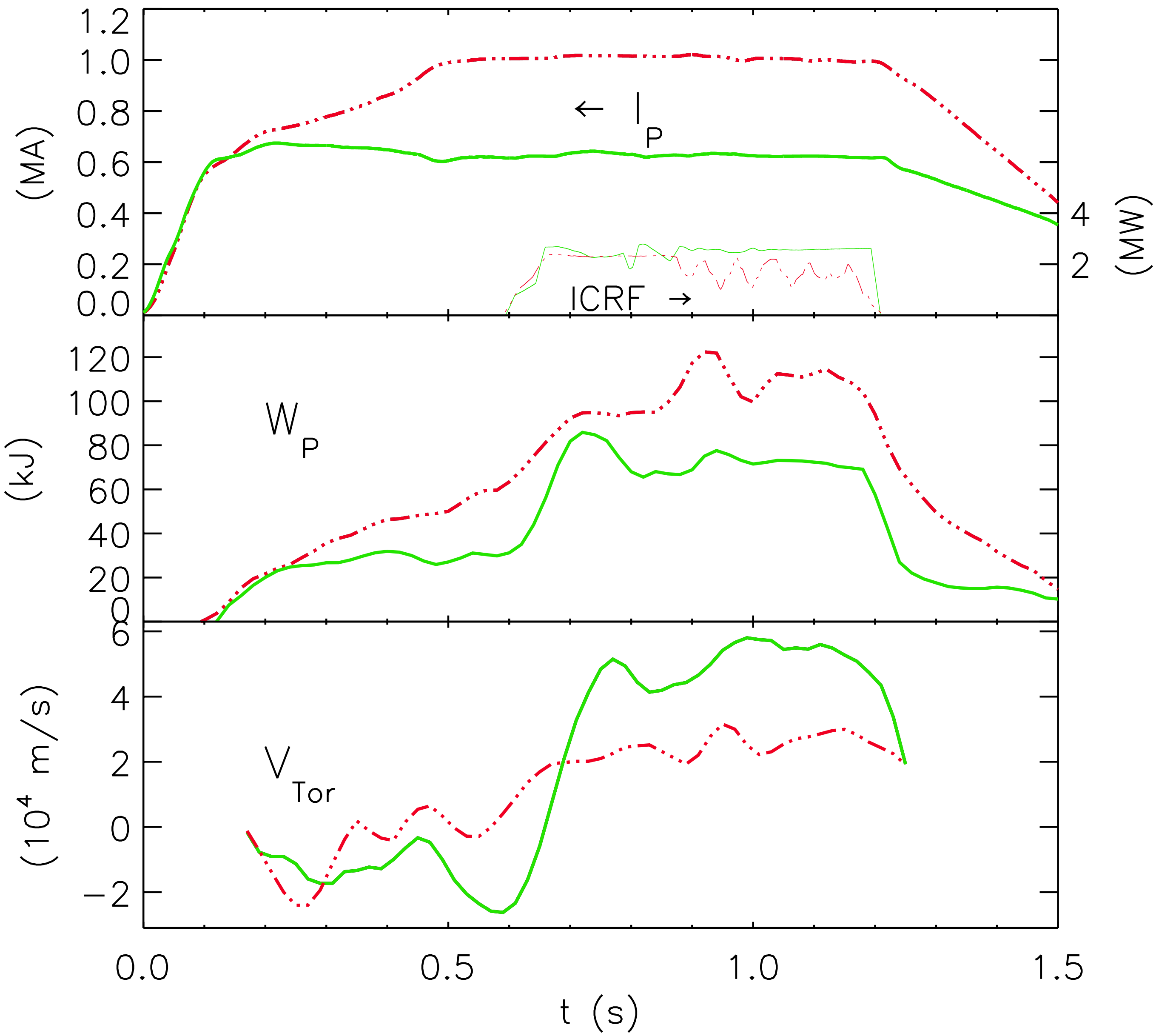

1.2
1.0
0.8
0.6
0.4
0.2
0.0
(MA)
← I_P
4
2
(MW)
ICRF →
120
100
80
60
40
20
0
(kJ)
W_P
6
4
2
0
−2
(10^4 m/s)
V_{Tor}
0.0
0.5
1.0
1.5
t (s)

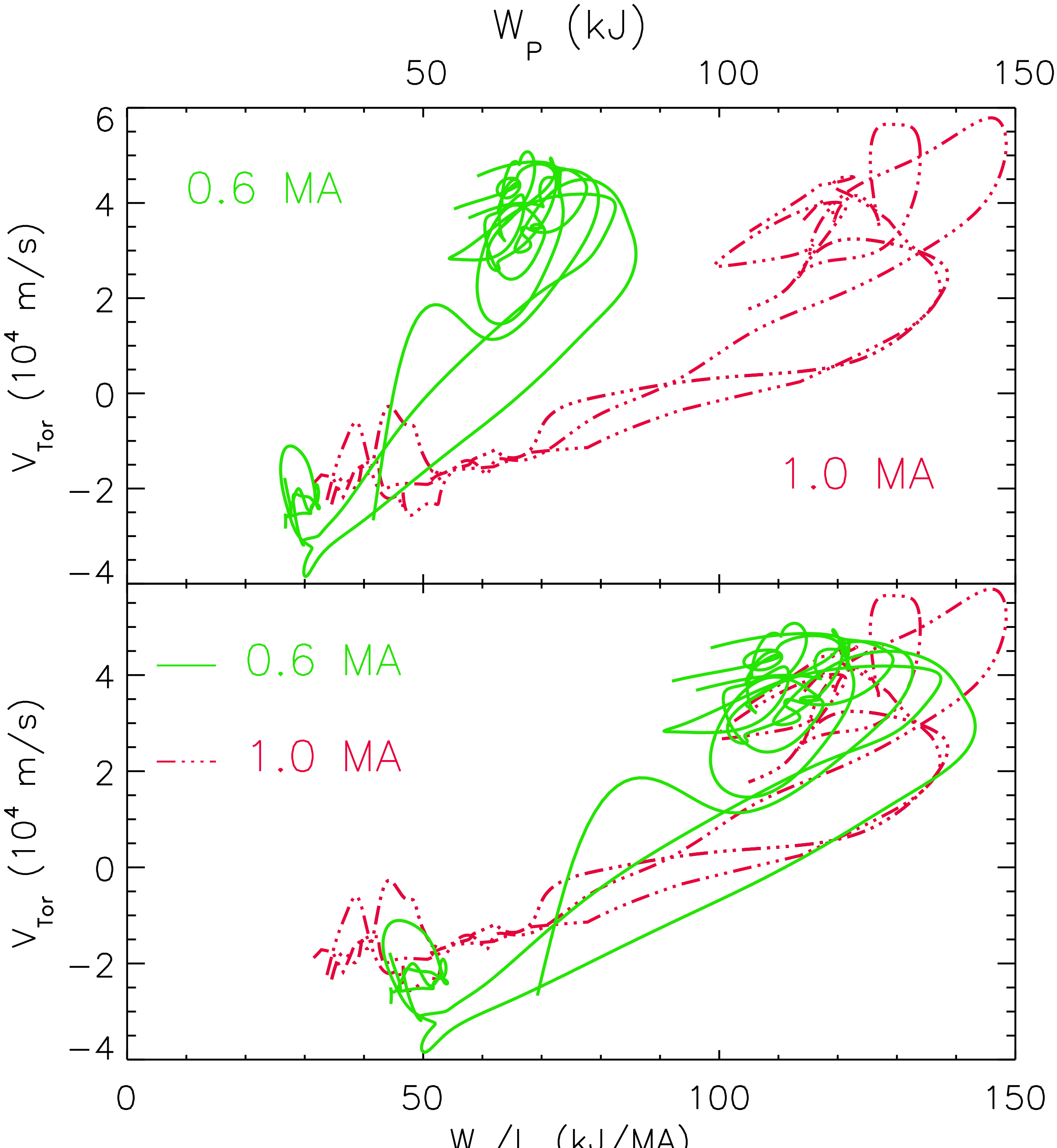

W_P (kJ)
50
100
150
6
4
2
0
−2
−4
0.6 MA
1.0 MA
V_Tor (10^4 m/s)
0.6 MA
1.0 MA
V_Tor (10^4 m/s)
0
50
100
150
W_P/I_P (kJ/MA)

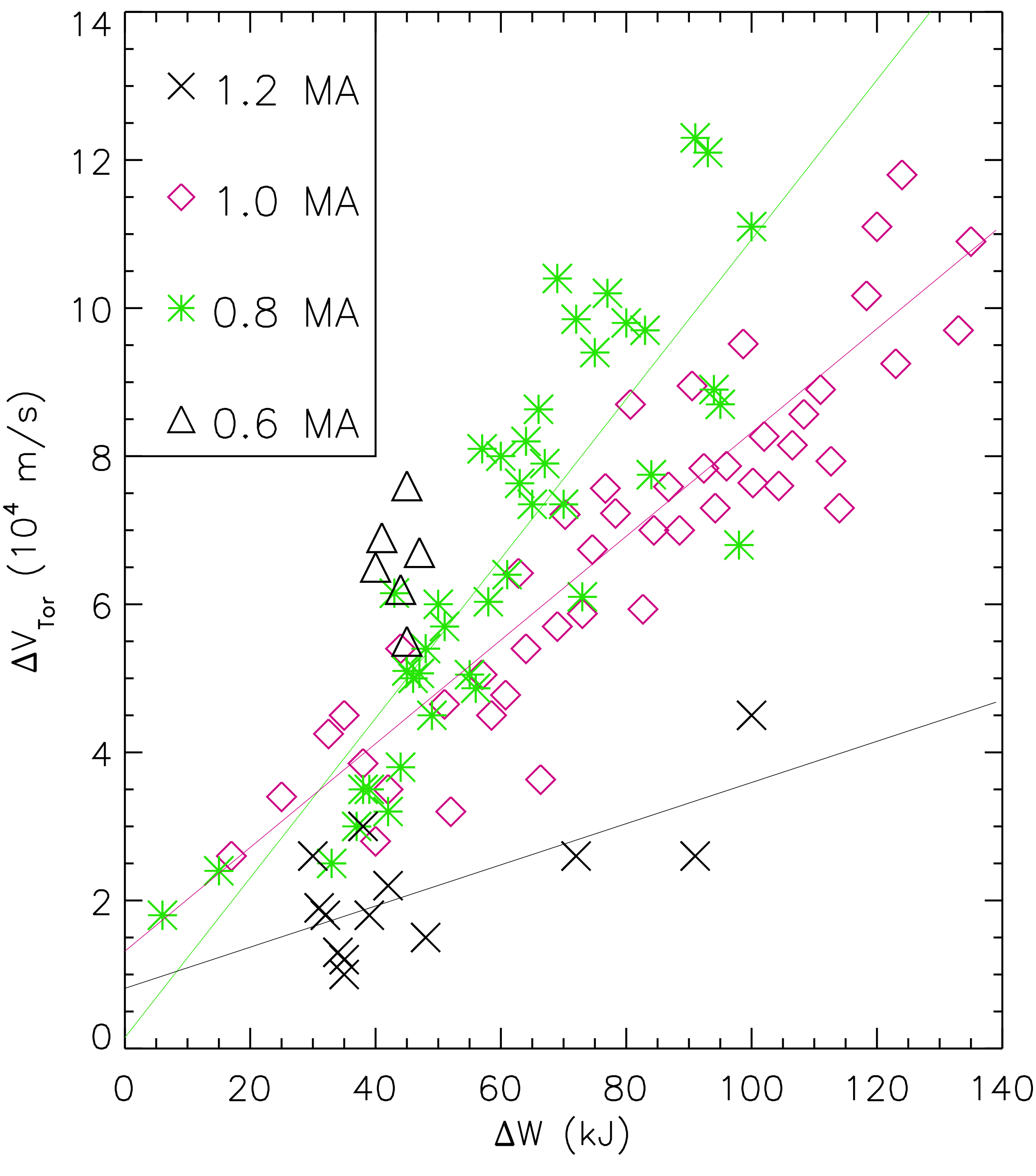

1.2 MA
1.0 MA
0.8 MA
0.6 MA
0
2
4
6
8
10
12
14
ΔV_Tor (10^4 m/s)
0
20
40
60
80
100
120
140
ΔW (kJ)

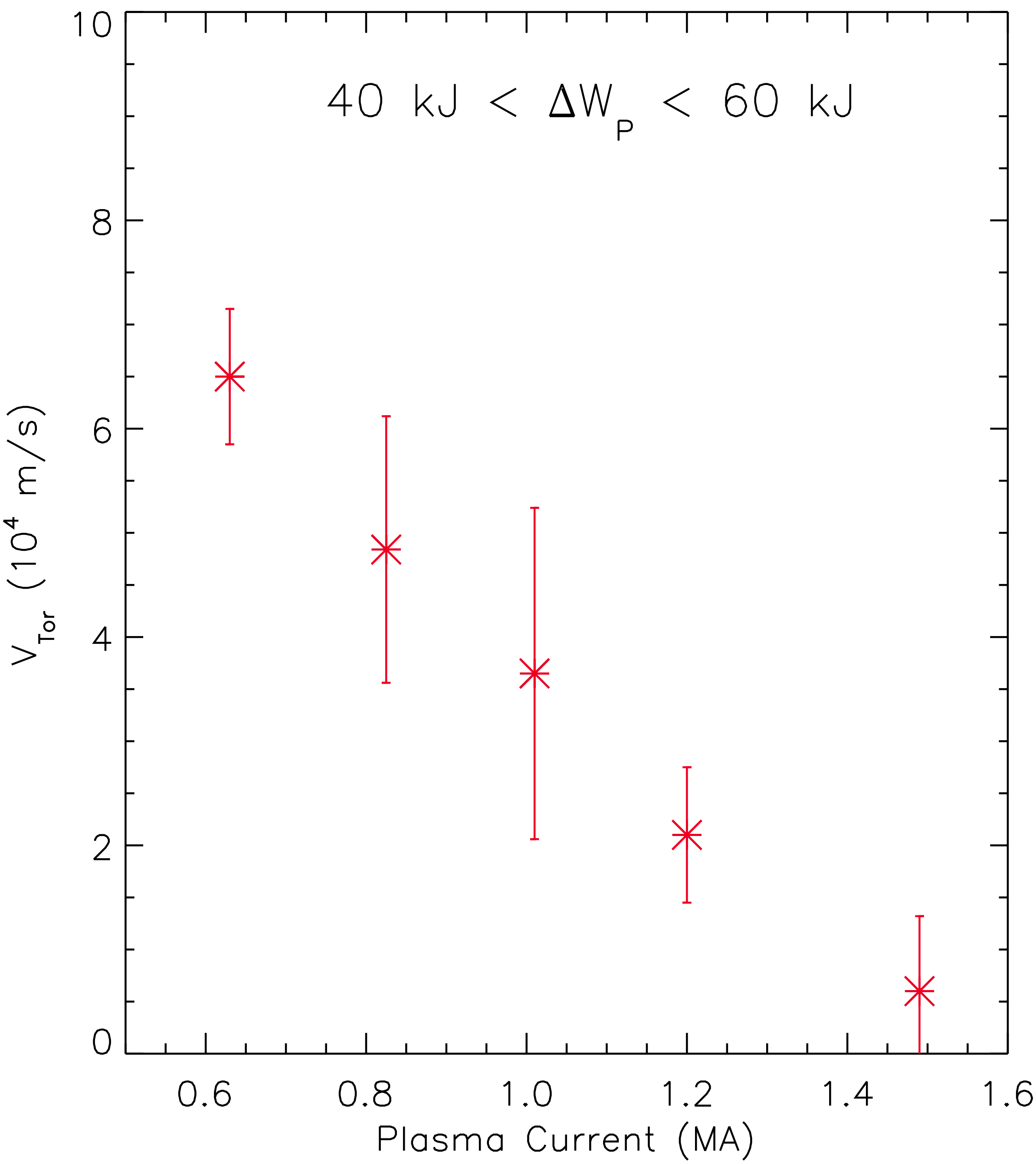

40 kJ < ΔW_P < 60 kJ
V_Tor (10^4 m/s)
Plasma Current (MA)
0
2
4
6
8
10
0.6
0.8
1.0
1.2
1.4
1.6

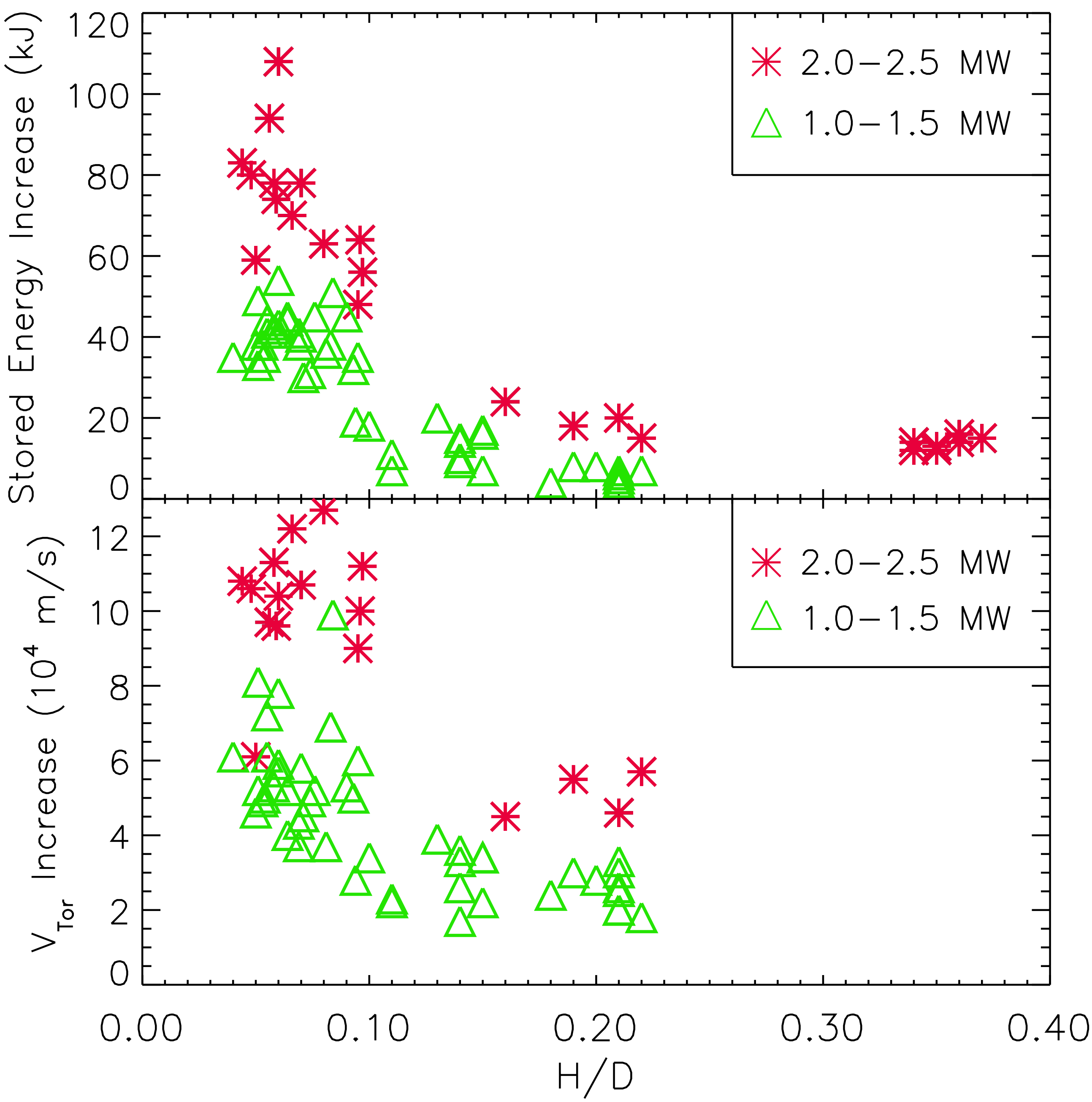

Stored Energy Increase (kJ)
120
100
80
60
40
20
0
2.0−2.5 MW
1.0−1.5 MW
V_{Tor} Increase (10^4 m/s)
12
10
8
6
4
2
0
2.0−2.5 MW
1.0−1.5 MW
0.00
0.10
0.20
0.30
0.40
H/D

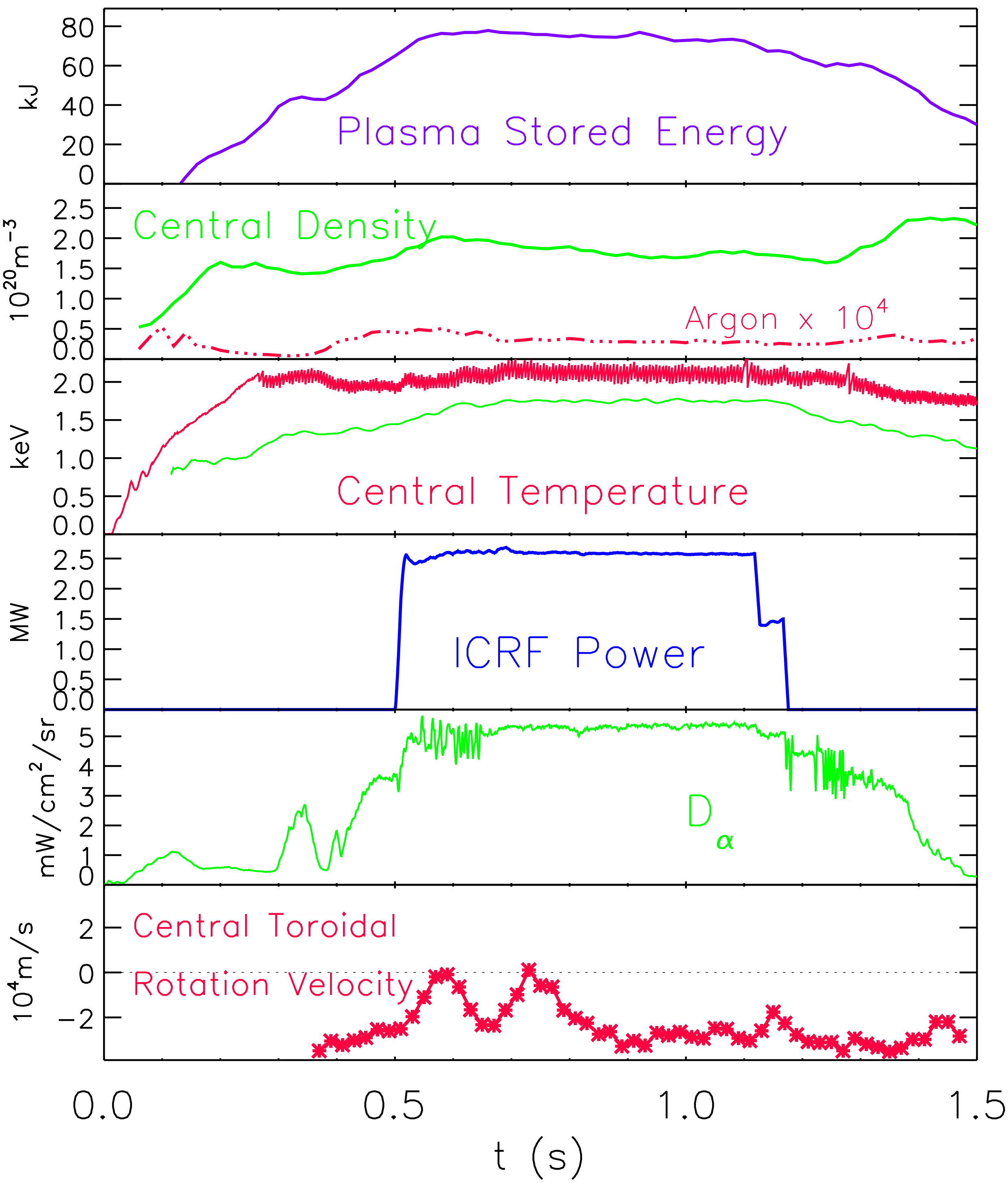

Plasma Stored Energy
kJ
80
60
40
20
0
Central Density
Argon x 10^4
$10^{20}m^{-3}$
2.5
2.0
1.5
1.0
0.5
0.0
Central Temperature
keV
2.0
1.5
1.0
0.5
0.0
ICRF Power
MW
2.5
2.0
1.5
1.0
0.5
0.0
D_α
$mW/cm^2/sr$
5
4
3
2
1
0
Central Toroidal
Rotation Velocity
$10^4 m/s$
2
0
−2
0.0
0.5
1.0
1.5
t (s)

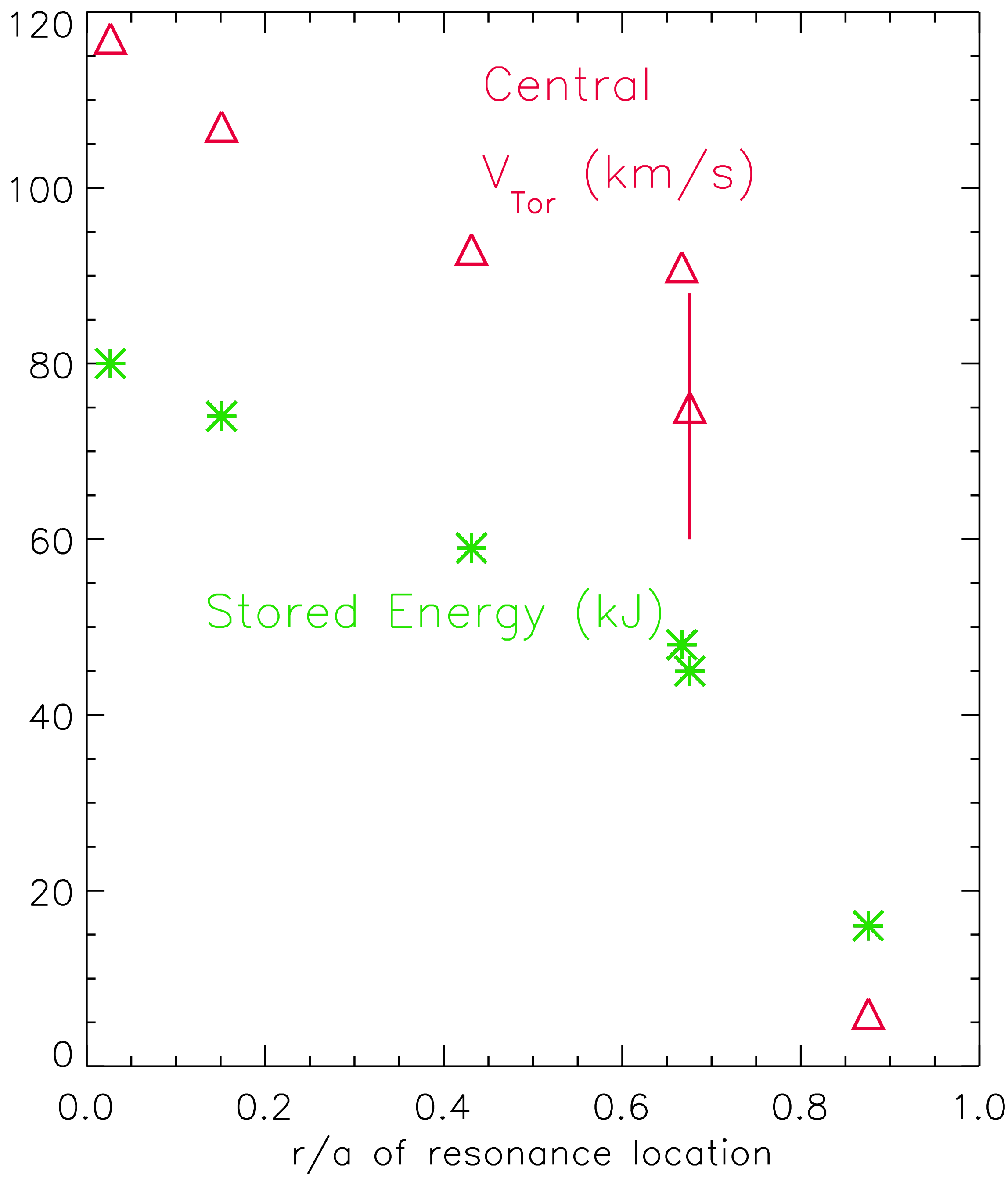

Central
V Tor (km/s)
Stored Energy (kJ)
120
100
80
60
40
20
0
0.0
0.2
0.4
0.6
0.8
1.0
r/a of resonance location

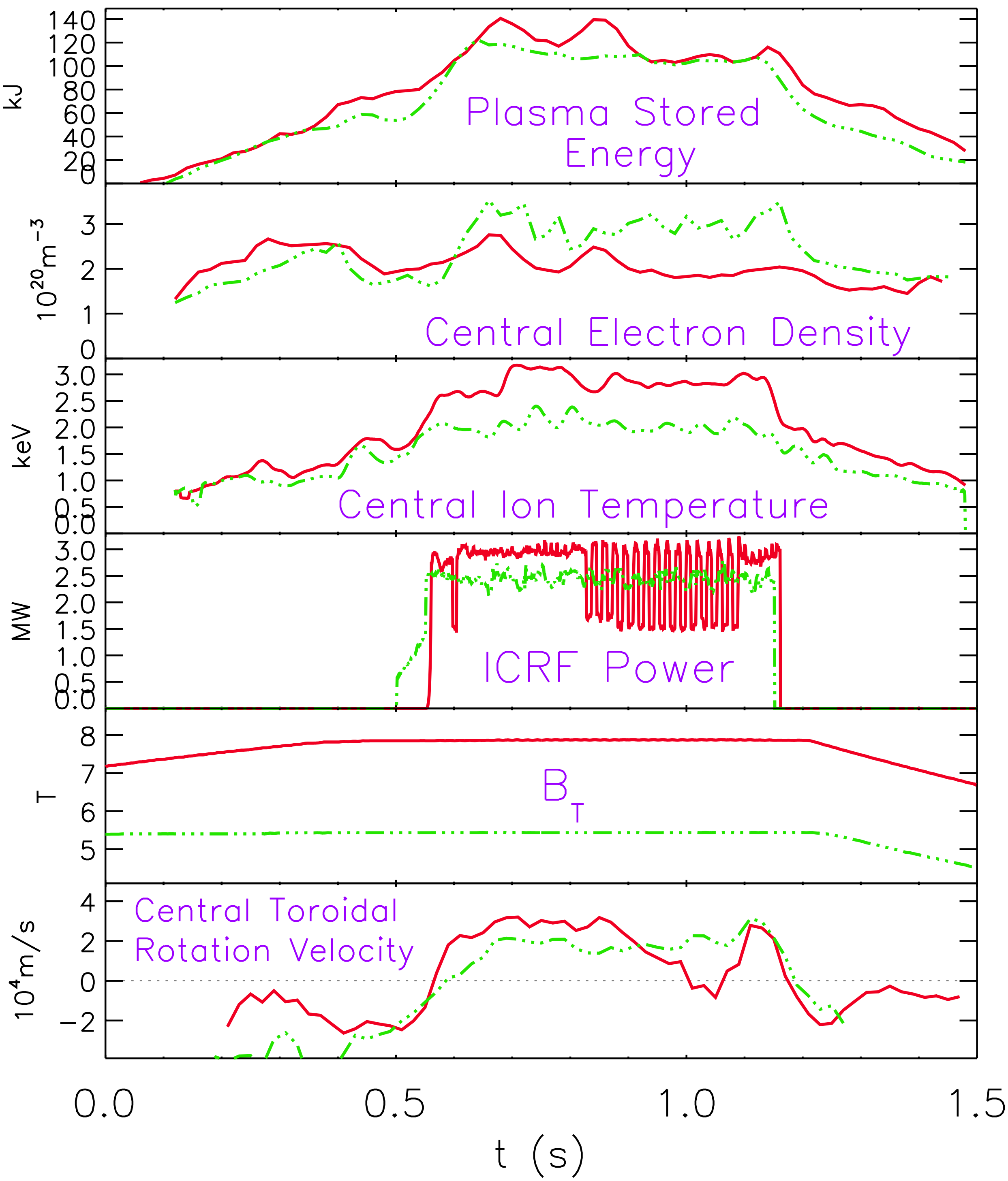

kJ
140
120
100
80
60
40
20
0
Plasma Stored
Energy
$10^{20}m^{-3}$
3
2
1
0
Central Electron Density
keV
3.0
2.5
2.0
1.5
1.0
0.5
0.0
Central Ion Temperature
MW
3.0
2.5
2.0
1.5
1.0
0.5
0.0
ICRF Power
T
8
7
6
5
B_T
10^4m/s
4
2
0
−2
Central Toroidal
Rotation Velocity
0.0
0.5
1.0
1.5
t (s)

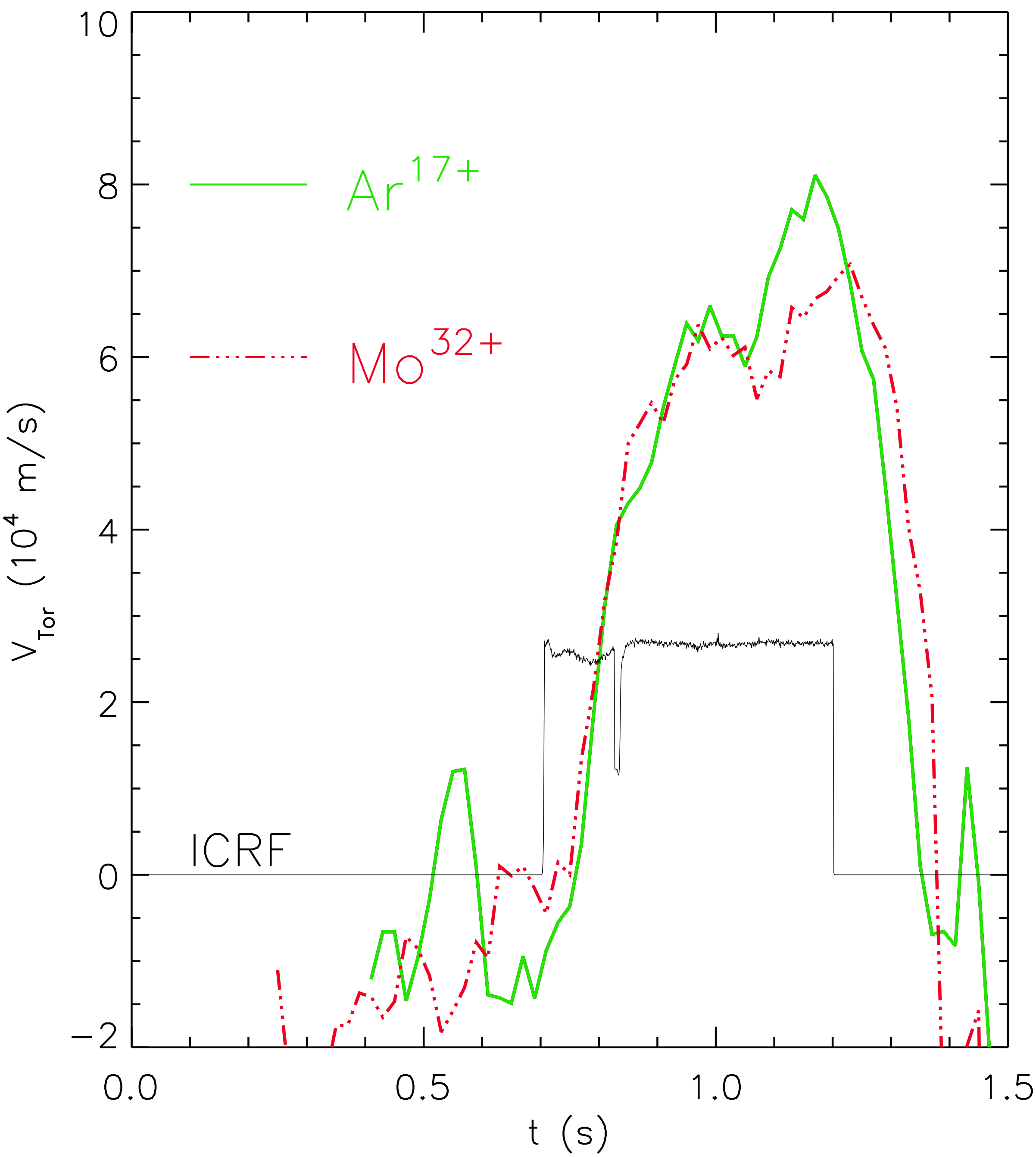

10
8
6
4
2
0
−2
0.0
0.5
1.0
1.5
t (s)
V_{Tor} (10^4 m/s)
Ar^{17+}
Mo^{32+}
ICRF

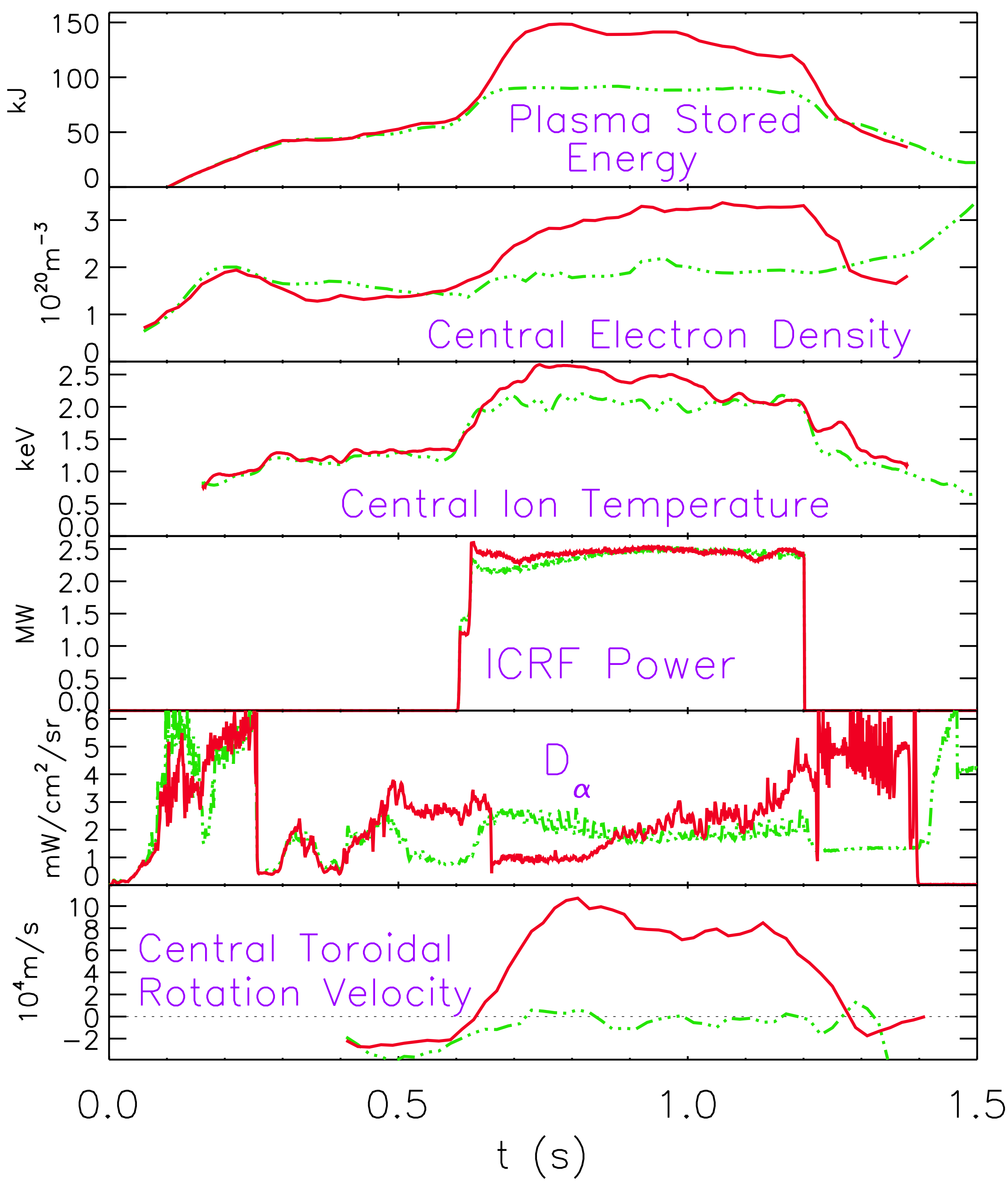

Plasma Stored Energy
kJ
150
100
50
0
Central Electron Density
$10^{20}m^{-3}$
3
2
1
0
Central Ion Temperature
keV
2.5
2.0
1.5
1.0
0.5
0.0
ICRF Power
MW
2.5
2.0
1.5
1.0
0.5
0.0
D_α
$mW/cm^2/sr$
6
5
4
3
2
1
0
Central Toroidal Rotation Velocity
$10^4m/s$
10
8
6
4
2
0
−2
0.0
0.5
1.0
1.5
t (s)

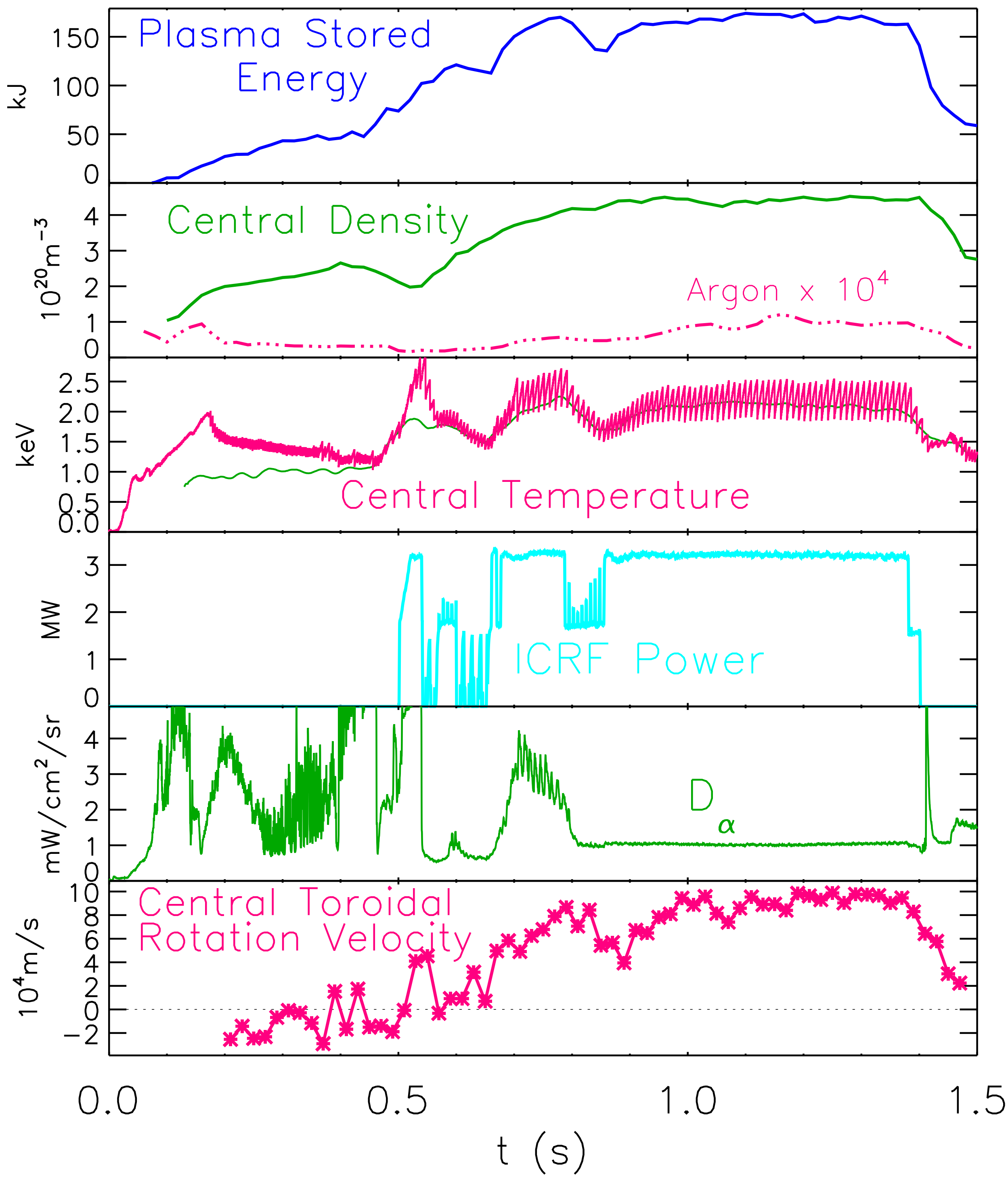

Plasma Stored Energy
kJ
150
100
50
0
Central Density
Argon x 10⁴
10²⁰m⁻³
4
3
2
1
0
keV
2.5
2.0
1.5
1.0
0.5
0.0
Central Temperature
MW
3
2
1
0
ICRF Power
mW/cm²/sr
4
3
2
1
0
Dα
Central Toroidal
Rotation Velocity
10⁴m/s
10
8
6
4
2
0
−2
0.0
0.5
1.0
1.5
t (s)

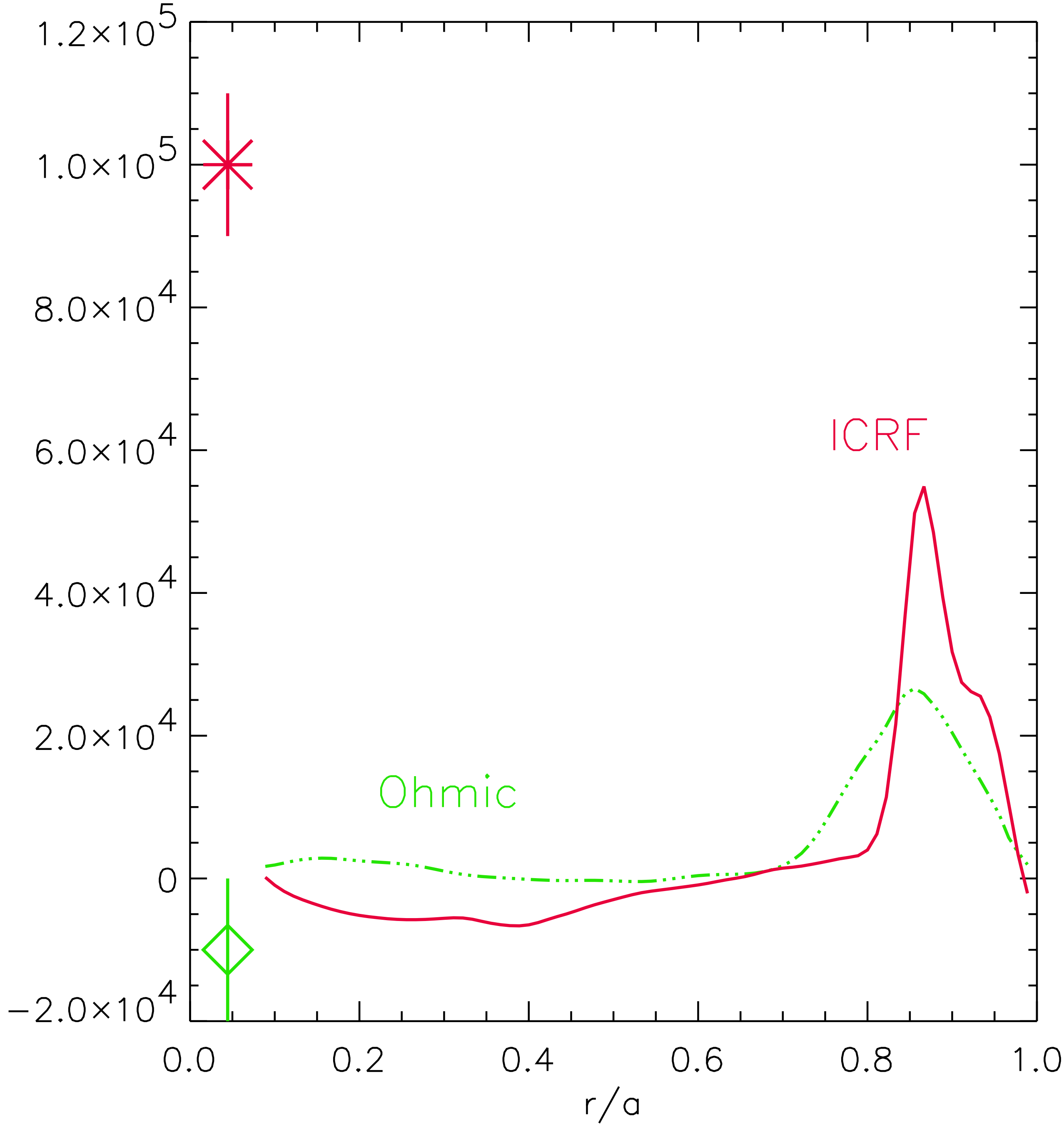

1.2×10^5
1.0×10^5
8.0×10^4
6.0×10^4
4.0×10^4
2.0×10^4
0
−2.0×10^4
V_Tor (m/s)
0.0
0.2
0.4
0.6
0.8
1.0
r/a
ICRF
Ohmic

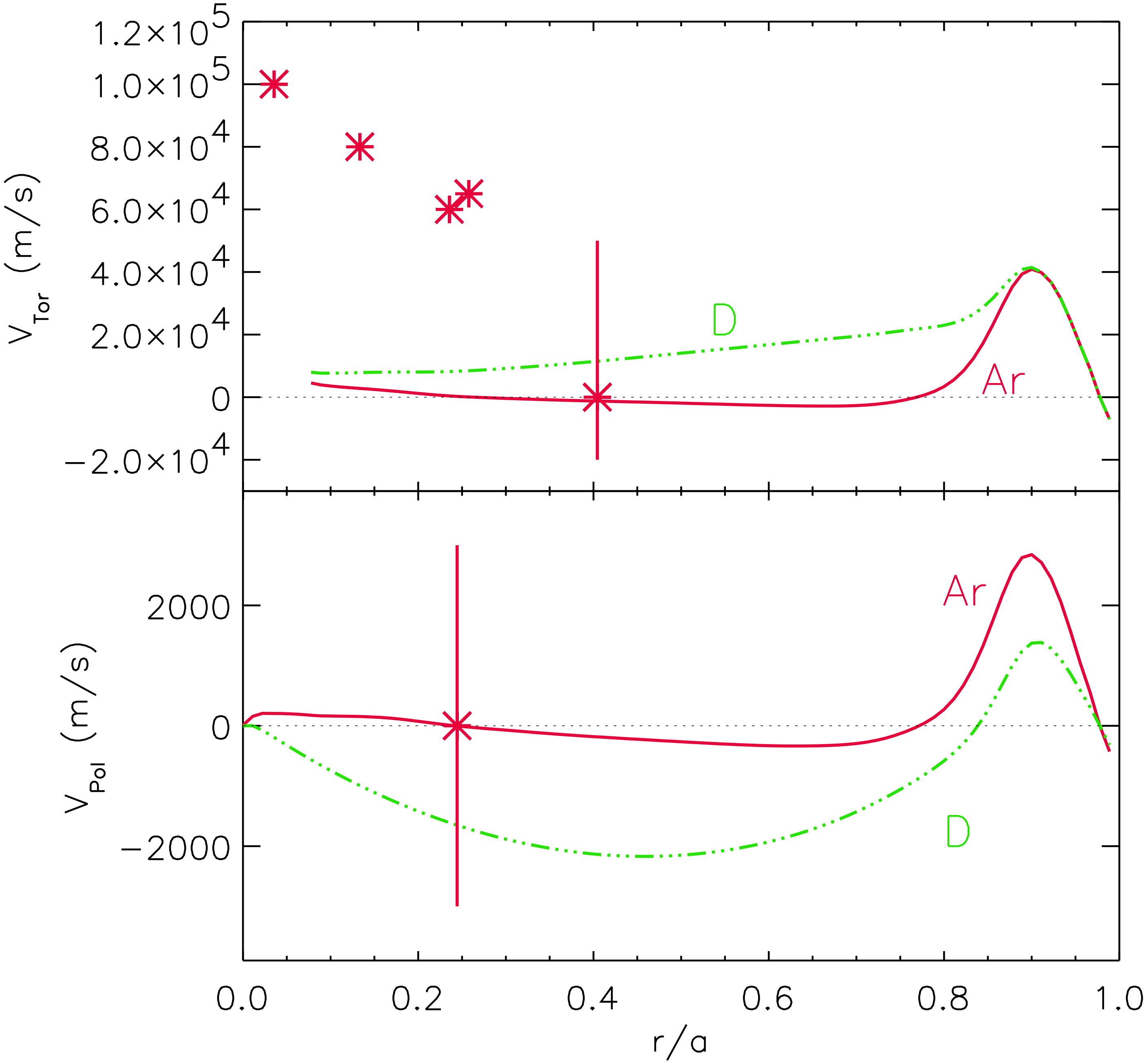

1.2×10^5
1.0×10^5
8.0×10^4
6.0×10^4
4.0×10^4
2.0×10^4
0
−2.0×10^4
V_Tor (m/s)
D
Ar
2000
0
−2000
V_Pol (m/s)
Ar
D
0.0
0.2
0.4
0.6
0.8
1.0
r/a